DOI: 10.1002/cmdc.200500024

Prediction of Small-Molecule Binding to Cytochrome P450 3A4: Flexible Docking Combined with Multidimensional QSAR

Markus A. Lill,* Max Dobler, and Angelo Vedani[a]

The inhibition of cytochrome P450 3A4 (CYP3A4) by small molecules is a major mechanism associated with undesired drug–drug interactions, which are responsible for a substantial number of late-stage failures in the pharmaceutical drug-development process. For a quantitative prediction of associated pharmacokinetic parameters, a computational model was developed that allows prediction of the inhibitory potential of 48 structurally diverse molecules. Based on the experimental structure of CYP3A4, possible binding modes were first sampled by using automated docking (Yeti software) taking protein flexibility into account. The results are consistent with both X-ray crystallographic data and data from metabolic studies. Next, an ensemble of energetically favorable orientations was composed into a 4D dataset for use as input for a multidimensional QSAR technique (Raptor software). A dual-shell binding-site model that allows an explicit induced fit was then generated by using hydrophobicity scoring and hydrogen-bond propensity. The simulation reached a cross-validated r^2 value of 0.825 and a predictive r^2 value of 0.659. On average, the predicted binding affinity of the training ligands deviates by a factor of 2.7 from the experiment; those of the test set deviate by a factor of 3.8 in K_i.

Introduction

During multi-drug medication, individual compounds may compete to be metabolized by the same enzyme(s). This can lead to undesired drug–drug interactions.[1] To assess toxic drug–drug interactions, a quantitative prediction of associated pharmacokinetic changes would be highly beneficial. The inhibition of biotransformations mediated by cytochrome P450 3A4 (CYP3A4) is considered to be a major mechanism of undesirable drug side-effects, as this enzyme is responsible for metabolizing 50–60% of orally administered drugs on the market, including anesthetics, antibiotics, steroids, and cancer chemotherapeutics.[2] Although CYP3A4 preferentially catalyzes the oxidation of lipophilic neutral or basic compounds, its active site—predominantly hydrophobic in nature—is capable of accommodating a wide range of structures, from simple and rigid steroids to macromolecules such as cyclosporins.

As the majority of drugs are metabolized by cytochrome P450 enzymes, the interactions of potential new therapeutics with CYP3A4 are typically characterized with in vitro screens as part of pharmaceutical research and development. This should facilitate the discovery and development of safer drugs with fewer side effects, minimal drug–drug interactions, and predictable pharmacokinetic properties. Virtual screening of new chemical entities for CYP3A4 binding could augment the pharmaceutical screening process by providing cost-effective information on metabolism and toxicity.

Herein we present a novel computational approach that combines flexible docking and multidimensional QSAR to screen for the inhibitory potential of small molecules. The X-ray crystal structures of various ligand–CYP complexes[3] demonstrate that water molecules play an essential role in ligand binding to CYP, and that induced protein fit may facilitate the binding process. Our computational approach takes both phenomena into account by including explicit water molecules "on-the-fly" during the docking process and by simulating local induced fit during flexible docking and multidimensional QSAR.

Computational Methods

Ligand data and molecular structure building

The structural and pharmacological data for 48 compounds (Figure 1) interacting with CYP3A4 as substrates or inhibitors were obtained from Wanchana and co-workers.[4] The inhibitory effect of these substances on the metabolism of 7-benzyloxy-4-trifluoromethylcoumarin were determined by using a competitive binding assay with recombinant CYP3A4 on a rapid microtiter plate as reported by Stresser et al.[5] All measured IC_{50} values were converted to K_i values with the Cheng–Prusoff relation.[6]

The 3D structures of all ligand molecules were generated with MacroModel 6.5[7] and optimized in hydrophobic solution (chloroform) with the AMBER* force field.[8] Atomic partial charges for the flexible docking study were computed by using the CM-1 methodology as implemented in the AMSOL package.[9]

[a] *M. A. Lill, M. Dobler, A. Vedani*
Biographics Laboratory 3R
Friedensgasse 35, 4056 Basel (Switzerland)
Fax: (+41) 61-2614258
E-mail: markus@biograf.ch

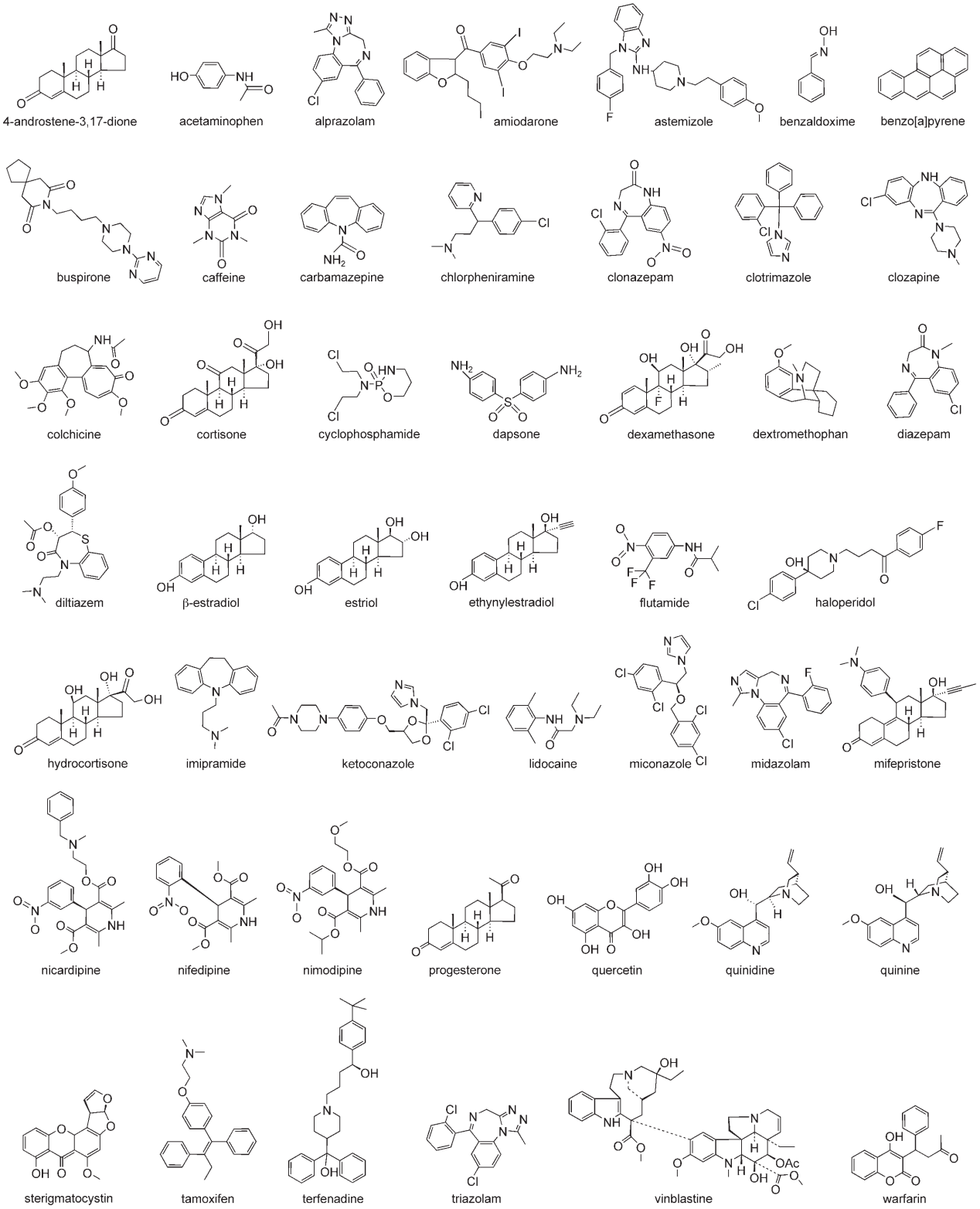

Figure 1. Structures of the 48 compounds that interact with CYP3A4 used in the receptor modeling study.

Docking

After completing the missing side chains of residues Lys 282, Glu 283, Thr 284, and Glu 285 (not resolved in the electron-density map) by using the PrGen software,[10] the X-ray crystal structure of the human CYP3A4 enzyme (PDB code: 1TQN), available at a resolution of 2.05 Å,[11] was relaxed by using energy refinement with Yeti 7.0[12] and molecular dynamics (MD) simulations with Amber 7.0.[13] The optimized structure was used as template for automatic docking of the individual

compounds by using Yeti. The iron–heme group was modeled in its oxenoid iron [Fe^{5+}···O^{2-}] form. The force field implemented in Yeti includes directional terms for hydrogen bonding and a metal function, which allows the simulation of charge transfer between iron, oxygen, and the heme nitrogen atoms.[14] The 6/12 van der Waals term between the oxygen atom of the oxenoid iron species and lipophilic, carbon-atom-containing groups of the ligand molecules was replaced by a specific 10/12 function ($r_0 = 3.0$ Å, $\varepsilon = -4.0$ kcal mol^{-1}) to allow close contacts, a prerequisite for complying with the metabolic capabilities of the enzyme.

As CYP3A4 can accommodate a wealth of different substrates (Figure 1), its binding pocket is rather wide and hydrophobic in nature. As a consequence, different binding modes and conformations must be considered for small molecules binding to it. Moreover, induced fit may facilitate ligand binding, accommodating compounds that differ as much as a factor of seven in their molecular volume. To identify the possible binding modes, we sampled structurally and energetically feasible arrangements within the binding pocket by using flexible docking combined with an extended Monte Carlo (MC) search protocol (Scheme 1) based on a Metropolis selection criterion (Yeti software)[12] and by allowing an adaptation of any protein side chain within 12 Å of the ligand molecule.[15]

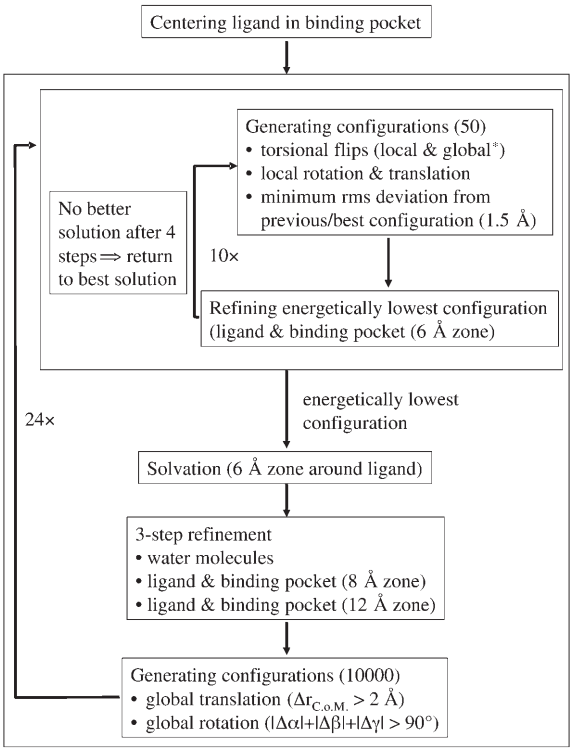

Scheme 1. Flexible docking protocol with an extended Monte Carlo search (* global means cis–trans flip for sp^2–sp^2 torsions, trans-gauche$^+$-gauche$^-$ for sp^3–sp^3 torsions).

After centering a compound in the binding pocket, 50 new ligand configurations were generated with local translation, rotation, and combined local/global torsion flips. The lowest-energy ligand–protein complex was refined and served as a template for the next MC step. The best previous configuration was restored if no lower-energy configuration was found after four MC trials. This permitted a global search without spending too much time in computation for local sampling of ligand configurations in unfavorable regions of the binding pocket. As X-ray crystal structures of various ligand–CYP complexes[3] have indicated that water molecules play an essential role in ligand binding to CYP, the lowest-energy structure of the complex that emerged from this first-pass MC was solvated and refined. An algorithm[16] previously developed for the systematic solvation of proteins based on the directionality of hydrogen bonds was used for solvating the docked complex. Finally, an extensive global search for new binding modes provided a new starting structure for a new first-pass MC run.

As some ligands are expected to have different binding modes as observed from the metabolic data,[17] and as even a directional force field[14] is not perfectly suited for scoring ligand–protein interactions, we retained and composed up to four energetically favorable protein–ligand arrangements (within 10 kcal mol^{-1} of the lowest-energy conformation) into a 4D data set in which each ligand is represented by different possible conformations, orientations, protonation states, or stereoisomers. This has been used as input for the multidimensional QSAR technology Raptor 2.0.[18]

Receptor modeling with multidimensional QSAR

Raptor,[18] a receptor-modeling concept developed by our research group, includes the possibility of representing each ligand molecule as an ensemble of conformations, orientations, stereoisomers, and protonation states (→4D QSAR), thereby decreasing the bias in identification of the bioactive conformer. In addition, it explicitly and anisotropically allows induced fit by a dual-shell representation of the 3D binding-site model, onto which the physicochemical properties (hydrophobicity and hydrogen-bonding propensity) are mapped. The inner shell is tailored by using the most potent ligand of the training set; the outer shell accommodates the topology of all molecules from the training set. The adaptation of both field and topology of the receptor surrogate to each ligand is carried out by combining a steric adjustment to the topology of the ligand in question and a component from the attraction or repulsion between ligand and receptor surrogate. The latter is obtained by correlating the physicochemical properties (hydrophobicity and hydrogen-bond propensity) of the ligand–receptor interaction in 3D space. As the mapping of properties onto the shells cannot be determined unambiguously (different models with similar predictive power can be identified), Raptor generates a family of receptor models. Such surrogate families may be interpreted to represent the various configuration states of the true biological receptor. The obtained binding affinities are averaged over the individual models (10 individual models throughout this work).

The underlying scoring function for evaluating ligand–protein interactions includes directional terms for hydrogen bonding (ΔG_{Hbond}), hydrophobicity (ΔG_{Hphob}), and terms for the cost of the topological adaptation (ΔG_{IF}) and changes in entropy

($T\Delta S$)[19] upon ligand binding:

$$\Delta G_{binding} = \Delta G_{constant} + \Delta G_{Hbond} + \Delta G_{HPhob} - T\Delta S + \Delta G_{IF} \quad (1)$$

Experimental determination of binding affinity for weak inhibitors is often prevented by limited solubility or limited sensitivity. Therefore, only an upper limit (or threshold, t_{UL}) for K_i values is accessible. These substances are typically neglected in QSAR studies, as no finite experimental binding affinity can be specified. However, these molecules contain valuable information about the receptor binding site: that is, the information that they do not bind strongly to the receptor. Particularly, for the purposes of lead-finding and for estimating the toxic potential of chemicals, a computational model should also be able to separate inhibitors of strong and moderate binding affinity from low-affinity and nonbinding compounds. Consequently, we extended the Raptor concept with a threshold option: the optimization algorithm forces the model to repro-

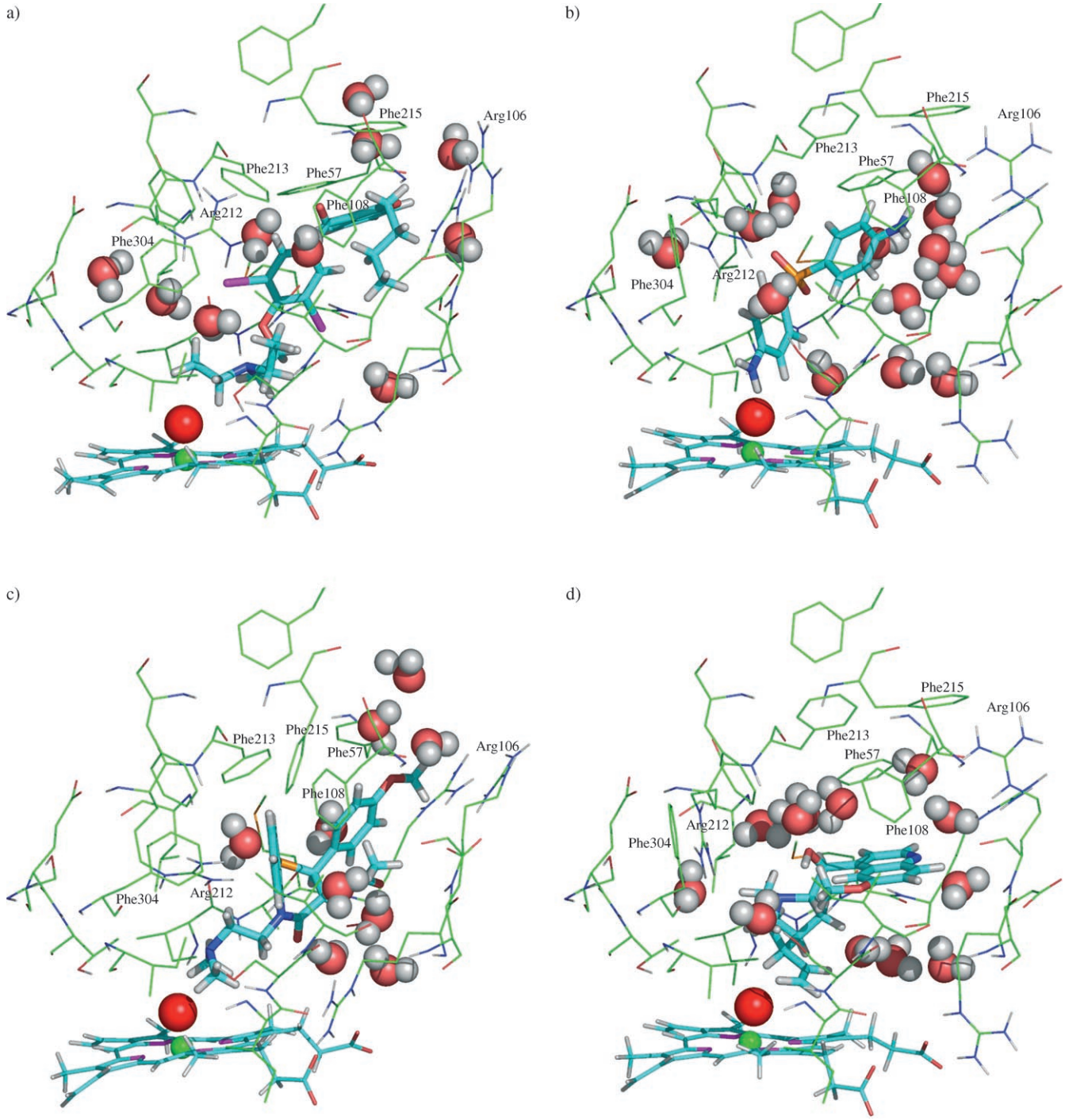

Figure 2. Low-energy configurations of a) amiodarone, b) dapsone, c) diltiazem, and d) quinine bound to CYP3A4 as determined by flexible docking. Color coding: oxygen = red, nitrogen = blue, carbon = cyan (ligand and heme) or green (protein), sulfur = orange, iodine = purple, hydrogen = white, iron = green.

duce the binding affinity of the low-affinity and nonbinding ligand molecules to be lower than the experimental limit. Clearly, no penalty is added to the lack-of-fit value for compounds which are experimentally measured to bind with an affinity lower than a threshold $K_i(t_{UL})$ value and which are correctly classified during the model optimization. If, on the other hand, the binding affinity of the ligand is predicted higher than the threshold value, the lack-of-fit function applies a penalty proportional to $\Delta G_{binding}(t_{UL}) - \Delta G_{binding}$.

Results and Discussion

Docking

To validate our docking approach against experimental findings, we targeted reproduction of the 3D structure of metyrapone bound to CYP3A4[20] as determined by X-ray crystallography. The second-lowest-energy arrangement identified by the docking procedure (Yeti software) reproduced the experimental structure within an root mean square of 0.2 Å. Two other configurations were found within 10 kcal mol^{-1} of the lowest-energy structure, both of which deviate further from experimental results. Of course, a single comparison is not sufficient for reliable validation. Owing to the limited crystallographic data on CYP3A4–ligand complexes (only metyrapone binds close to the heme group), an indirect validation scheme was chosen by checking our docking results for consistency against experimental metabolism data on CYP3A4.

Figure 2 shows low-energy structures of amiodarone, dapsone, diltiazem, and quinine as obtained by flexible docking. Each appears to be in agreement with known metabolism data (Figure 3).[21] The lowest-energy complex of CYP3A4 with amiodarone (Figure 2a) is formed with ethyl group of the bound drug in close proximity to the heme oxygen atom ($C_{ethyl}\cdots O_{heme}$ distance = 3.0 Å); de-ethylation is considered to be the dominant metabolic reaction of CYP3A4 on amiodarone (Figure 3). The energetically most favorable complex of dapsone with CYP3A4 (Figure 2b; $N_{anilinic}\cdots O_{heme}$ distance = 2.7 Å) agrees with experimental results in which the metabolic reaction of CYP3A4 on dapsone is N-hydroxylation (Figure 3). Diltiazem is N-demethylated (Figure 3); the second-lowest-energy docking configuration (Figure 2c; $C_{tert\text{-}amine}\cdots O_{heme}$ distance = 2.9 Å) is also consistent with experimental results. In the energetically most favorable complex of CYP3A4 with quinine (Figure 2d), the hydrogen atom at the 3 position points toward the heme oxygen atom ($C3\cdots O_{heme}$ distance = 3.0 Å) in agreement with the observed 3-hydroxylation reaction of CYP3A4 (Figure 3).

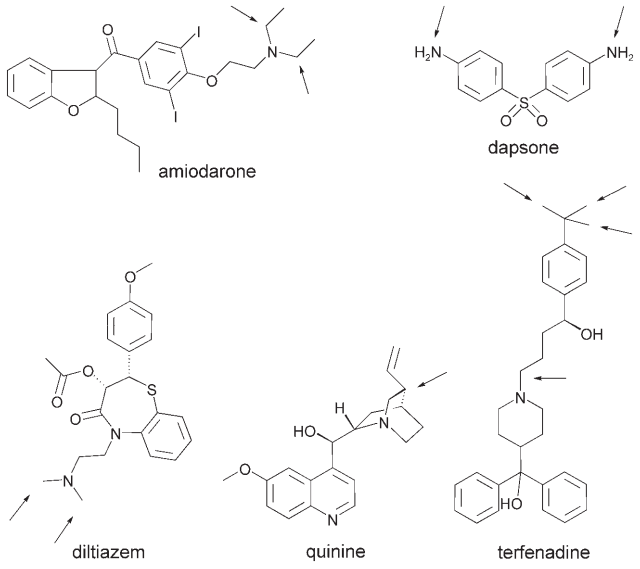

Figure 3. Structures of amiodarone, dapsone, diltiazem, quinine, and terfenadine; arrows indicate the positions of biotransformation by CYP3A4 as determined experimentally.[17,21]

Figure 2 also indicates the significance of induced protein fit and water molecules upon ligand binding to CYP3A4. Whereas Arg 212 is hydrogen bonded to the backbone carbonyl oxygen atom of Ile 369 in the amiodarone–CYP3A4 complex (Figure 2a), Arg 212 alters its conformation upon diltiazem binding (Figure 2c) to engage in a hydrogen bond with the cyclic thioether sulfur atom of diltiazem. Phe 304 is found in two different configurations: an "out" position in the quinine–CYP3A4 complex, in which Phe 304 provides space for four water molecules to accommodate the hydroxy group of quinine (Figure 2d), and an "in" position in the diltiazem–CYP3A4 complex, in which Phe 304 forms a π–π interaction with the benzene portion of the heterocyclic ring of diltiazem (Figure 2c). The four complexes also display the flexibility of a phenylalanine cluster composed of residues 57, 108, 213, and 218 by adapting to the topology of the ligand present.

Several water molecules are likely to bind to the active site to stabilize the ligand–CYP3A4 complexes. They either reflect stripped water molecules surrounding the hydrophilic groups of the ligands in the hydrophobic portion of the binding pocket (Figure 2a: accommodating the carbonyl and ether groups of amiodarone; Figure 2c: the methoxy oxygen atom; Figure 2d: the hydroxy group of quinine), or are engaged as hydrogen-bond mediators between ligand and protein (Figure 2b: linking the amine group of dapsone with the side chain nitrogen atom and the backbone carbonyl oxygen atom of Arg 106, and between the sulfonyl group of dapsone with Arg 212; Figure 2c: between the ester group of diltiazem and Glu 374).

Figure 4 displays a further example of the low-energy docking configurations of terfenadine. In the lowest-energy configuration (Figure 4a), two of the three *tert*-butyl methyl groups are located 3.0 Å from the heme oxygen atom. In the third-lowest configuration (Figure 4a) the two CH_2 groups vicinal to the piperidyl nitrogen atom are 3.0 Å and 4.3 Å apart from the heme oxygen atom. This is in agreement with available metabolism data (Figure 3), which suggests that terfenadine is metabolized to terfenadine alcohol or azacyclonol.[17] This also demonstrates that different binding modes of the ligand at hand are consistent with the present metabolism data, and that several distinct low-energy complex structures in our docking approach have to be taken into account for quantifying ligand–protein interactions. Consequently, the different

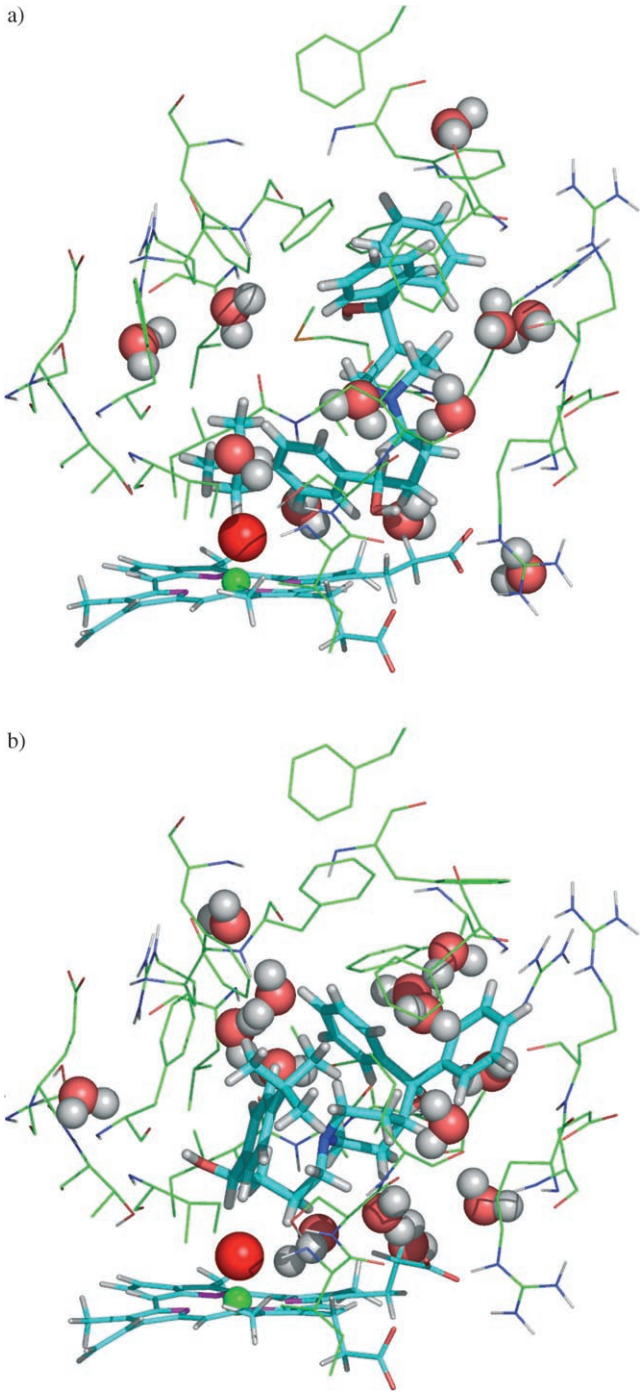

Figure 4. a) Lowest-energy and b) third-lowest-energy configurations of terfenadine bound to CYP3A4 as determined by flexible docking. Color coding: oxygen = red, nitrogen = blue, carbon = cyan (ligand and heme) or green (protein), hydrogen = white, iron = green.

low-energy ligand orientations have been composed in a 4D data set and were used as input for the multidimensional QSAR technology Raptor[18] to give 192 representations for the 48 molecules.

Table 1. Predicted versus experimentally determined binding affinities.

Ligand	Name	pK_i^{exptl}	pK_i^{calcd}	ΔpK_i
	Test set			
1	acetaminophen	3.30	3.60	0.30
2	amiodarone	6.22	6.68	0.46
3	buspirone	5.13	4.86	0.27
4	clonazepam	4.25	3.62	0.63
5	imipramine	4.44	3.83	0.62
6	mifepristone	6.64	5.79	0.85
7	quinidine	4.60	3.93	0.67
8	warfarin	3.98	4.82	0.84
9	caffeine	<3.08	1.48	n/a
10	estriol	<4.77	5.58	n/a
	Training set			
11	4-androstene-3,17-dione	3.78	4.58	0.80
12	alprazolam	3.85	4.51	0.66
13	astemizole	5.97	6.30	0.33
14	benzaldoxime	3.92	3.74	0.18
15	carbamazepine	3.90	4.58	0.68
16	chlorpheniramine	3.63	4.25	0.62
17	clotrimazole	7.95	7.38	0.57
18	clozapine	4.99	5.45	0.46
19	colchicine	4.19	4.75	0.56
20	cyclophosphamide	5.22	4.37	0.85
21	dapsone	4.57	4.10	0.47
22	dextromethophan	4.48	4.71	0.23
23	diazepam	4.42	4.43	0.02
24	diltiazem	4.58	4.02	0.56
25	β-estradiol	4.91	4.96	0.05
26	ethynylestradiol	6.11	5.98	0.13
27	haloperidol	4.71	5.28	0.57
28	ketoconazole	8.52	8.34	0.18
29	lidocaine	3.31	2.72	0.60
30	miconazole	6.80	6.59	0.21
31	midazolam	5.93	5.11	0.82
32	nicardipine	6.89	6.62	0.27
33	nifedipine	5.26	4.79	0.47
34	nimodipine	6.12	6.00	0.12
35	progesterone	4.82	4.40	0.42
36	quercetin	5.18	5.02	0.16
37	quinine	4.72	4.11	0.61
38	sterigmatocystin	6.19	5.55	0.64
39	tamoxifen	5.60	5.66	0.06
40	terfenadine	5.91	6.36	0.45
41	triazolam	4.27	5.11	0.85
42	verapamil	6.04	6.02	0.01
43	vinblastine	5.24	5.79	0.55
44	benzo(a)pyrene	<5.52	5.67	n/a
45	cortisone	<4.00	4.46	n/a
46	dexamethasone	<3.48	3.89	n/a
47	flutamide	<3.78	3.86	n/a
48	hydrocortisone	<3.18	3.91	n/a

Receptor modeling with multidimensional QSAR

Our multidimensional QSAR study (software Raptor) was based on 48 structurally diverse molecules (Table 1): 38 defined the training set and 10 defined the test set. For seven compounds, only an upper limit for their K_i values was experimentally determined; these molecules defined the "threshold class" (five in the training set, two in the test set). Induced fit was taken into account by the dual-shell concept of Raptor. To allow topological and physicochemical variation at the true biological receptor with different ligands bound, the Raptor results were averaged over 10 individual models defining a surrogate family.

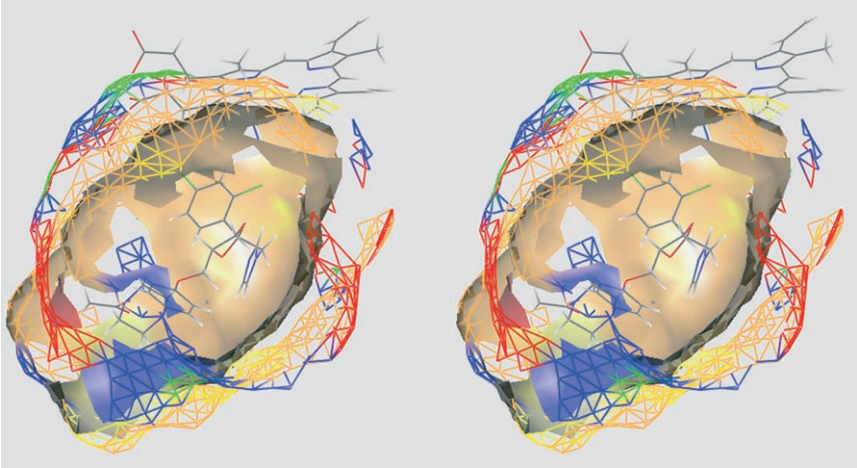

Figure 5. Stereo representation of the CYP3A4 binding-site model with ketoconazole bound, as generated by the Raptor technology (hydrophobic fields = beige, hydrogen-bond-donating propensity = blue, hydrogen-bond-accepting propensity = red, hydrogen-bond flip-flop = green). The inner shell (solid surface) and outer shell (wire frame) are shown in different style to highlight the two shells of the receptor model. Only the properties common among the 10 individual models are displayed.

The simulation reached a cross-validated r^2 value of 0.825 (with a leave-group-out protocol consisting of five groups) and yielded a predictive r^2 value of 0.659. The binding-site model is depicted in Figure 5. Comparison with the enzyme crystallographic structure (Figures 2 and 4) shows the predominantly hydrophobic character of the binding pocket (represented by Phe 57, Phe 74, Val 81, Phe 108, Ile 120, Phe 213, Phe 215, Leu 216, Phe 241, Ile 301, Phe 304, Val 393, and Leu 482). The hydrogen-bonding moieties (H-bond acceptors that mimic the carboxylate group of Glu 374 and the backbone carbonyl oxygen atoms of Phe 213 and Arg 106, and H-bond donors that mimic the guanidinium groups of Arg 106, Arg 212 and Arg 372) are also well-identified by the model. Experimental and calculated K_i values are compared in Figure 6 and Table 1. On average, the predicted binding affinity of the training ligands deviates by a factor 2.7 from the experimental result; those of the test set deviate by a factor 3.8 in K_i. The maximum observed deviations of an individual molecule are 7.0 (training) and 7.1 (test)—a respectable result, as the test set includes diverse molecules that are not similar in structure to any compound of the training set. All low-affinity and nonbinding molecules were predicted to bind with affinities close to or weaker than the experimental threshold value. Therefore, the model appears to be able to separate these molecules from the class of strong inhibitors. A series of five scramble tests[22] (mean predictive $r^2 = 0.276$) demonstrated the sensitivity of the model family toward the biological data.

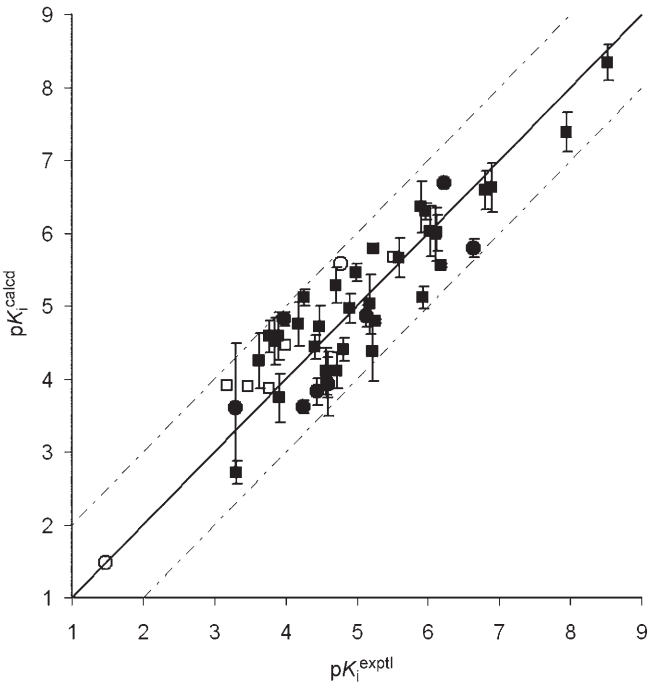

Figure 6. Predicted versus experimental binding affinities for ligand molecules bound to CYP3A4: training set (■), test set (●); threshold compounds: training set (□), test set (○). Error bars represent variations of the prediction over the 10 individual models.

Analysis of the energetic contributions (Equation (1) and Figure 7) suggests that hydrophobic interactions are dominant for most ligand molecules in our study: ΔG_{HPhob} varies from -1.7 kcal mol^{-1} for the hydrophilic compound quercetin to -12.2 kcal mol^{-1} for the most affine molecule ketoconazole. Averaging over all compounds, ΔG_{HPhob} (-6.9 kcal mol^{-1}) dominates the contribution of ΔG_{HBond} (-0.9 kcal mol^{-1}) by a factor of eight. However, our analysis indicates that direct and water-mediated hydrogen-bond interactions may play a significant role for selected compounds: ΔG_{HBond} approximates ΔG_{HPhob} for dapsone ($\Delta G_{HBond} = -3.3$ kcal mol^{-1}), ethynylestradiol (-4.0 kcal mol^{-1}) and even dominates for quercetin (-5.7 kcal mol^{-1}), consistent with the docking results (Figure 2b, dapsone). The entropy component $T\Delta S$ associated with the freezing of a the rotational degrees of freedom for a given ligand and the energetic cost for induced protein fit (although smaller in absolute magnitude) contributes significantly to the difference in free energy of ligand binding as well. The binding affinity of the rather flexible molecule terfenadine, for example, is lowered by 2.3 kcal mol^{-1} as a result of the loss of rotational entropy.

Conclusions

Our virtual model for the quantitation of small-molecule binding affinities for CYP3A4 combines flexible docking and multidimensional QSAR, and indicates a significant potential to

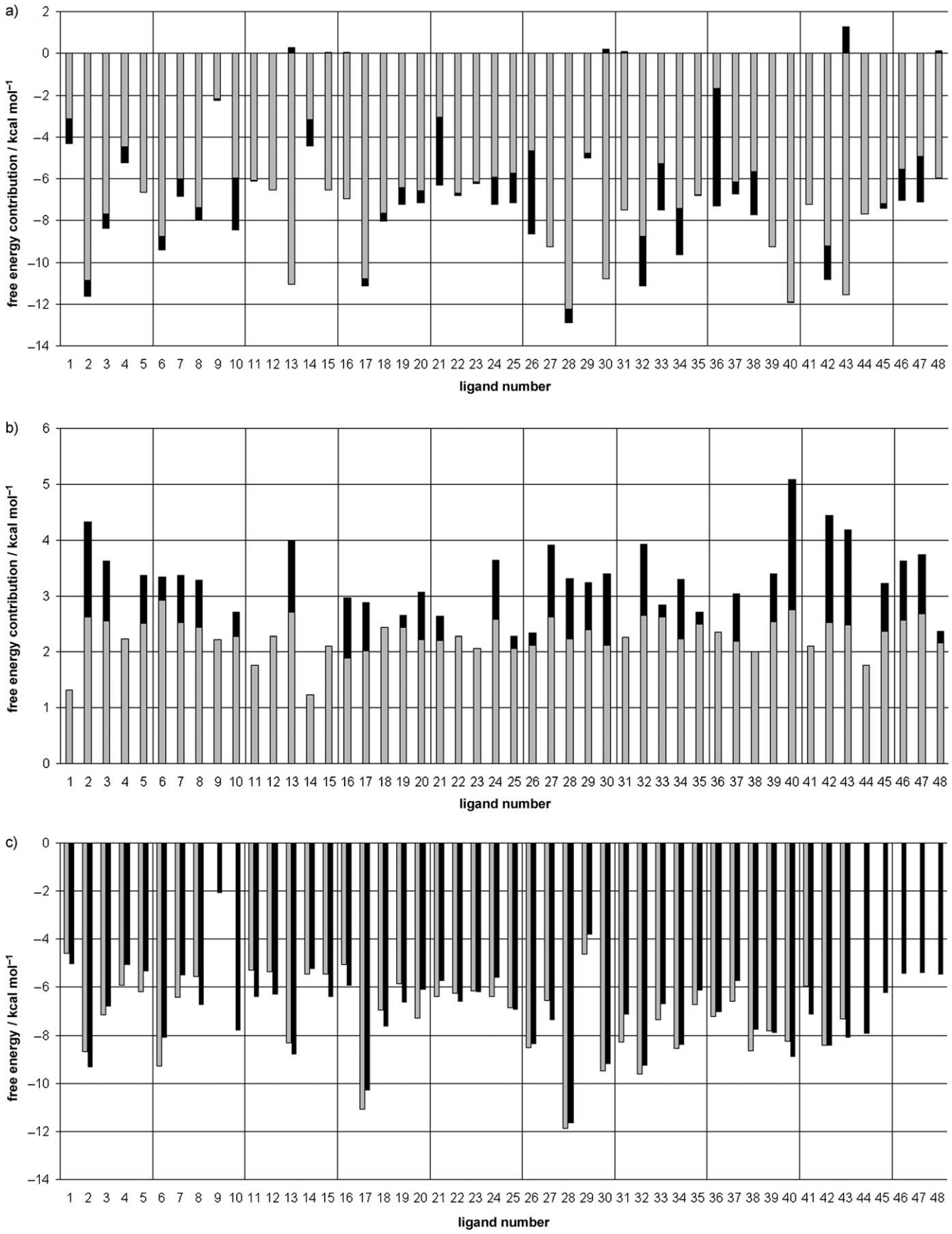

Figure 7. Free-energy contributions: a) hydrophobic (gray) and hydrogen-bonding interactions (black); b) cost for induced fit (gray) and entropy (black); c) experimental (gray) versus predicted (black) free energies of binding. The ligand numbering corresponds to that in Table 1.

screen new or hypothetical compounds for binding to CYP3A4 and, indirectly, for possible drug–drug interactions. Our docking approach was validated against an experimentally determined complex structure (X-ray crystallography) and known metabolism data on CYP3A4 for a total of five structurally diverse compounds. The consistency of the docking results with the experimental metabolism data suggests that our procedure may also be used to propose realistic binding modes of novel compounds. The approach could track down biologically relevant interactions with the metabolic active center (iron-bound heme) and could subsequently identify active metabolites of existing or new hypothetical ligands. Analysis of the results show that induced protein fit and water molecules that bridge ligand and protein are essential for small-molecule binding to CYP3A4. Both features have been explicitly simulated in docking (Yeti software) and model-building experiments (Raptor software). The study further indicates that besides hydrophobic contacts, hydrogen-bonding and water-mediated hydrogen-bonding interactions play an important role in ligand–CYP3A4 interactions.

Keywords: ADMET · cytochromes · drug–drug interactions · molecular modeling · structure–activity relationships

[1] E. J. Tanaka, *J. Clin. Pharm. Ther.* **1998**, *23*, 403 – 416.
[2] F. P. Guengerich, *Adv. Pharmacol.* **1997**, *43*, 7 – 35.
[3] a) M. R. Wester, J. K. Yano, G. A. Schoch, C. Yang, K. J. Griffin, C. D. Stout, E. F. Johnson, *J. Biol. Chem.* **2004**, *279*, 35 630 – 35 637; b) P. A. Williams, J. Cosme, A. Ward, H. C. Angove, D. M. Vinkovic, H. Jhoti, *Nature* **2003**, *424*, 464 – 468; c) M. R. Wester, E. F. Johnson, C. Marques-Soares, S. Dijols, P. M. Dansette, D. Mansuy, C. D. Stout, *Biochemistry* **2003**, *42*, 9335 – 9345; d) O. Pylypenko, I. Schlichting, *Annu. Rev. Biochem.* **2004**, *73*, 991 – 1018.
[4] S. Wanchana, F. Yamashita, M. Hashida, *Pharm. Res.* **2003**, *20*, 1401 – 1408.
[5] D. M. Stresser, A. P. Blanchard, S. D. Turner, J. C. L. Erve, A. A. Dandeneau, V. P. Miller, C. L. Crespi, *Drug Metab. Dispos.* **2000**, *28*, 1440 – 1448.
[6] H. C. Cheng, *J. Pharmacol. Toxicol. Methods* **2001**, *46*, 61 – 71.
[7] F. Mohamadi, N. G. J. Richards, W. C. Guida, R. Liskamp, M. Lipton, C. Caufield, G. Chang, T. Hendrickson, W. C. Still, *J. Comput. Chem.* **1990**, *11*, 440 – 467.
[8] S. J. Weiner, P. A. Kollman, D. A. Case, U. C. Singh, C. Ghio, G. Alagona, S. Profeta, Jr., P. Weiner, *J. Am. Chem. Soc.* **1984**, *106*, 765 – 784.
[9] C. J. Cramer, D. G. Truhlar, *J. Comput.-Aided Mol. Des.* **1992**, *6*, 629 – 666.
[10] P. Zbinden, M. Dobler, G. Folkers, A. Vedani, *Quant. Struct.-Act. Relat.* **1998**, *17*, 122 – 130.
[11] J. K. Yano, M. R. Wester, G. A. Schoch, K. J. Griffin, C. D. Stout, E. F. Johnson, *J. Biol. Chem.* **2004**, *279*, 38 091 – 38 094.
[12] http://www.biograf.ch/PDFS/Yeti.pdf.
[13] a) D. A. Case, D. A. Pearlman, J. W. Caldwell, T. E. Cheatham III, J. Wang, W. S. Ross, C. L. Simmerling, T. A. Darden, K. M. Merz, R. V. Stanton, A. L. Cheng, J. J. Vincent, M. Crowley, V. Tsui, H. Gohlke, R. J. Radmer, Y. Duan, J. Pitera, I. Massova, G. L. Seibel, U. C. Singh, P. K. Weiner, P. A. Kollman, AMBER 7, University of California, San Francisco, **2002**; b) The simulation was performed under periodic boundary conditions by using Ewald summation. After solvating the protein by using a water box with dimensions to ensure a distance of at least 8 Å from any protein atom to the box boundary, the system was minimized. The water molecules were then equilibrated by slowly heating from 100 to 500 K and cooling down again to 300 K. The same procedure was repeated for the whole system, followed by an equilibration period of 200 ps at a constant temperature of 300 K. Finally, the system was minimized to give a refined structure that deviated by only 1.3 Å from the experimental X-ray crystallographic structure.
[14] A. Vedani, A. , D. W. Huhta, *J. Am. Chem. Soc.* **1990**, *112*, 4759 – 4767.
[15] Depending on the size of the ligand molecule, each of the 48 docking simulations required 30 min–8 h of CPU time on a Macintosh G5 computer (2.5 GHz). The method is thus aimed at predicting the potential for drug–drug interactions of compounds already identified as possible lead structures.
[16] A. Vedani, D. W. Huhta, *J. Am. Chem. Soc.* **1990**, *112*, 5860 – 5862.
[17] K.-H. J. Ling, G. A. Leeson, S. D. Burmaster, R. H. Hook, M. K. Reith, L. K. Cheng, *Drug Metab. Dispos.* **1995**, *23*, 631 – 636.
[18] a) M. A. Lill, A. Vedani, M. Dobler, *J. Med. Chem.* **2004**, *47*, 6174 – 6186; b) http://www.biograf.ch/PDFS/Raptor.pdf.
[19] M. S. Searle, D. H. Williams, *J. Am. Chem. Soc.* **1992**, *114*, 10 690 – 10 697.
[20] P. A. Williams, J. Cosme, D. M. Vinkovic, A. Ward, H. C. Angove, P. J. Day, C. Vonrhein, I. J. Tickle, H. Jhoti, *Science* **2004**, *305*, 683 – 686.
[21] a) G. Fabre, B. Julian, B. Saint-Aubert, H. Joyeux, Y. Berger, *Drug Metab. Dispos.* **1993**, *21*, 978 – 985; b) D. Sutton, A. M. Butler, L. Nadin, M. Murray, *J. Pharmacol. Exp. Ther.* **1997**, *282*, 294 – 300; c) Y. Irshaid, A. Adedoyn, M. Lotze, R. A. Branch, *Drug Metab. Dispos.* **1994**, *22*, 161 – 164; d) X.-J. Zhao, H. Yokoyama, K. Chiba, S. Wanwimolruk, T. Ishizaki, *J. Pharmacol. Exp. Ther.* **1996**, *279*, 1327 – 1334.
[22] a) A. Vedani, M. Dobler, *J. Med. Chem.* **2002**, *45*, 2139 – 2149; b) http://www.biograf.ch/PDFS/Quasar.pdf; c) A. Vedani, M. Dobler, M. A. Li, *J. Med. Chem.* **2005**, *48*, 3700 – 3703.

Received: August 16, 2005
Published online on October 27, 2005

